

Prompt muon-induced fission: a sensitive probe for nuclear energy dissipation and fission dynamics

Volker E. Oberacker and A. Sait Umar

Department of Physics & Astronomy, Vanderbilt University,
Nashville, TN 37235, USA

Feodor F. Karpeshin

St. Petersburg State University, RU-198504 St. Petersburg, Russia
Dept. Physics, Univ. of Coimbra, P-3004-516 Coimbra, Portugal

July 24, 2018

Abstract

Following the formation of an excited muonic atom, inner shell transitions may proceed without photon emission by inverse internal conversion, i.e. the muonic excitation energy is transferred to the nucleus. In actinides, the $2p \rightarrow 1s$ and the $3d \rightarrow 1s$ muonic transitions result in excitation of the nuclear giant dipole and giant quadrupole resonances, respectively, which act as doorway states for fission. The nuclear excitation energy is typically 6.5 – 10 MeV. Because the muon lifetime is long compared to the timescale of prompt nuclear fission, the motion of the muon in the Coulomb field of the fissioning nucleus may be utilized to learn about the dynamics of fission. If there is large friction between the outer fission barrier and the scission point the muon will remain in the lowest molecular energy level and emerge in the $1s$ bound state of the heavy fission fragment. On the other hand, if friction is small (i.e. the nuclear collective motion is fast) there is a nonvanishing probability that the muon may be promoted to higher-lying molecular orbitals, e.g. the $2p\sigma$ level, from where it will end up attached to the light fission fragment. Therefore, theoretical studies of the muon-attachment probability to the light fission fragment, P_L , in combination with experimental data can be utilized to analyze the dynamics of fission, and nuclear energy dissipation in particular. In this way, one may be able to distinguish between nuclear energy dissipation arising from two-body collisions and “one-body friction” caused by the mean field. We study the dynamics of a muon bound to a fissioning actinide nucleus in two different ways: first, we solve the non-relativistic time-dependent Schrödinger equation using the Born-Oppenheimer expansion method in terms of quasimolecular wavefunctions. In the second approach, we solve the relativistic time-dependent Dirac equation on a 3-D Cartesian lattice utilizing the B-Spline collocation method. For $^{237}_{93}\text{Np}$ we find a dissipated energy of order 0 – 10 MeV and a fission time delay due to friction of up to $2 \cdot 10^{-21}$ s.

1 Introduction

Nuclear physics experiments with μ^- beams provide information on fundamental symmetries and interactions. Muonic atoms, in particular, have proven extremely useful in examining the electromagnetic properties of nuclei, e.g. electric charge distributions and multipole moments, because the muon has a high position probability density inside the nucleus owing to its small Compton wavelength $\lambda_c = \hbar/(m_\mu c) = 1.87\text{ fm}$ [1]. After muons have been captured into high-lying single particle states they form an excited muonic atom. Inner shell transitions may proceed without photon emission by inverse internal conversion [2], i.e. the muonic excitation energy is transferred to the nucleus. In actinides, the $E1 : (2p \rightarrow 1s, 6.6\text{ MeV})$ and the $E2 : (3d \rightarrow 1s, 9.5\text{ MeV})$ muonic transitions result in excitation of the nuclear giant dipole and giant quadrupole resonances, respectively, which act as doorway states for fission. Following these atomic transitions, the muon will be in the ground state of the actinide atom and can be utilized to probe the fission dynamics. Finally though, the muon is going to be captured by one of the fission fragments. However, nuclear capture as a result of the weak interaction occurs on a time scale of order 10^{-7} s which is many orders of magnitude larger than the time scale of fission.

From a theoretical point of view, prompt muon-induced fission has several attractive features. Because the nuclear excitation energy equals or exceeds the fission barrier height it is permissible to treat the fission dynamics classically (no barrier tunneling). The muon dynamics is determined by the electromagnetic interaction which is precisely known; hence, the process can be calculated, at least in principle, with any desired precision. Our main task is the solution of the Dirac equation for the muon in the presence of a time-dependent external Coulomb field which is generated by the fission fragments in motion.

We will demonstrate that the muon attachment to the light fission fragment depends on the nuclear friction between the outer fission barrier and the scission point. In this context, nuclear friction is defined as the irreversible flow of energy (and linear or angular momentum) from collective to intrinsic single-particle motion[3]. We include in our classical dynamical calculations for the fission mode a linear friction force to account for energy dissipation via neutron and photon emission. Through muon-induced fission one expects to gain a deeper understanding of the energy dissipation mechanism in large-amplitude nuclear collective motion.

The prompt muon-induced fission process is most easily understood via a “correlation diagram”, i.e. one plots the single-particle energies of the transient muonic molecule as a function of the internuclear distance (see Fig.3 of ref.[4]). If there is a large amount of friction during the motion from the outer fission barrier to the scission point the muon will remain in the lowest molecular energy level $1s\sigma$ and emerge in the $1s$ bound state of the *heavy* fission fragment. If, on the other hand, friction is small and hence the nuclear collective motion is relatively fast there is a

nonvanishing probability that the muon may be promoted to higher-lying molecular orbitals, e.g. the $2p\sigma$ level, from where it will end up attached to the *light* fission fragment. Therefore, theoretical studies of the muon-attachment probability to the light fission fragment, P_L , in combination with experimental data can be utilized to analyze the dynamics of fission, and nuclear energy dissipation in particular.

There are two different mechanisms that contribute to nuclear energy dissipation: two-body collisions and “one-body friction”. The latter is caused by the moving walls of the self-consistent nuclear mean field. The role played by these two dissipation mechanisms in fission and heavy-ion reactions is not yet completely understood. In 1976, in a pioneering work Davies, Sierk and Nix [5] calculated the effect of viscosity on the dynamics of fission. Assuming that friction is caused by two-body collisions they extracted a viscosity coefficient $\mu = 0.015$ Tera Poise from a comparison of theoretical and experimental values for the kinetic energies of fission fragments. The corresponding time delay for the nuclear motion from the saddle to the scission point was found to be of order $\Delta t = 1 \times 10^{-21}$ s. However, in one-body dissipation models the time delay is an order of magnitude larger.

Theoretical studies in combination with rather scarce experimental data on prompt fission obtained so far give rise to a definite answer: Estimates of the energy dissipated in the case of the one-body mechanism were made in the two-center harmonic oscillator model in analytical form [6]. For this purpose, the Born-Oppenheimer expansion method developed for calculation of the muon promotion probability, was applied for assessment of the nucleon promotion rate to higher quasimolecular orbitals, arising from the translation of the nascent fragments. The last process provides the microscopic mechanism for the one-body dissipation. The obtained estimate of the dissipated energy, $E_{diss} < 1\text{MeV}$, allows one to rule out the one-body mechanism, even with all the approximations of the model kept in mind.

Several experimental techniques are sensitive to the energy dissipation in nuclear fission. At high excitation energy, the multiplicity of pre-scission neutrons [7] or photons [8] depends on the dissipation strength. At low excitation energy, the process of prompt muon-induced fission [9] provides a suitable “clock”. This process will be discussed here.

Nonrelativistic calculations for muon-induced fission have been carried out by several theory groups, starting in 1980 [9, 10, 11, 12, 13], but relativistic calculations using the Dirac equation for the muon only became feasible in 1992 [14, 4, 15, 16]. We discuss here in detail our theoretical approach and the numerical implementation, and we compare our results with experimental data obtained at the Los Alamos Meson Physics Facility (LAMPF) [17, 18], at the Tri-University Meson Facility (TRIUMF) [19, 20], and at CERN and the Paul Scherrer Institute (PSI) [21, 22, 23, 24, 25].

2 Prompt and Delayed Fission Induced by Muons

Following the irradiation of a target with a μ^- beam the muons lose most of their kinetic energy by ionization in the target material within 10^{-9} to $10^{-10}s$. Once their velocity has become comparable to the orbital electron velocities characteristic of these atoms, they are slowed down further by inelastic collisions with valence electrons and are finally captured into high-lying states ($n_\mu \approx 14$) forming a muonic atom. The theoretical aspects of the interaction of muons with condensed matter were first studied by Fermi and Teller [26] and were later explored in more detail by Wu and Wilets [27] and by Kim [1]. Because all muonic bound states are unoccupied the muon will cascade down to the ground state within $10^{-13}s$. From the outer shells the excited muonic atom decays preferentially by emission of Auger electrons. Since ΔE increases rapidly for the inner shells, the transitions between levels with $n \leq 5$ are dominated by mesic X-rays. Alternatively, the transitions may proceed without emission of radiation via inverse internal conversion. From the K-shell, the muon disappears at a characteristic rate $\lambda = \lambda_0 + \lambda_c$, where $\lambda_0 = (2.2 \times 10^{-6}s)^{-1}$ denotes the free leptonic decay rate and λ_c the nuclear capture rate; λ_c depends upon the charge and mass of the nucleus (Goulard-Primakoff formula [28]) and is of order $(7.5 \times 10^{-8}s)^{-1}$ for actinides [18]. Muons stopped in an actinide target may induce nuclear fission in two different ways:

- *Delayed Fission Following Nuclear Muon Capture*

The muon is captured by a proton inside the nucleus and forms a neutron and a muon neutrino

$$\mu^- + (Z, A) \rightarrow (Z - 1, A)^* + \nu_\mu. \quad (1)$$

Even though most of the energy is taken away by the neutrino, the average nuclear excitation energy is $15 - 20\text{MeV}$ which is well above the fission barrier for actinides $E_f = 5 - 6\text{MeV}$. Fission via nuclear muon capture is *delayed*, i.e. it occurs with the characteristic mean lifetime of the weak decay process, $\tau_{capt} = (7 - 8) \times 10^{-8}s$.

- *Prompt Fission Resulting From Inverse Internal Conversion In Muonic Atoms*

In this case, the excitation energy of the muonic atom is transferred to the nucleus by an internal conversion process (nonradiative transition) and the muon ends up in the K-shell of the muonic atom

$$(Z, A)(\mu^-)^* \rightarrow (Z, A)^* \mu^-. \quad (2)$$

For the innermost atomic transitions in an actinide muonic atom, the transition energy generally exceeds the fission barrier height. The result is *prompt fission in the presence of the muon*, since the muon is not annihilated by this process, in contrast to fission resulting from nuclear muon capture. The nucleus will be surrounded by the muon during the entire fission process, unless the muon is ionized. Eventually, the muon will decay by nuclear muon capture from the fission fragments.

Experimentally, both fission modes can be distinguished because of their different time scale. In this paper, we focus on prompt muon-induced fission. This process was first discussed by Wheeler [29] and considered in more detail by Zaretski and Novikov [30]. It is important to know the specific atomic transitions that are responsible for prompt fission. Fig.1 of ref.[4] shows the Coulomb interaction energy between the muon and a ^{238}U nucleus as well as the binding energies of the lowest bound states. Even though E0 transitions such as $2s \rightarrow 1s$ and $3s \rightarrow 1s$ exhibit the largest internal conversion rates they do not contribute to fission because they lead to excitation of the giant monopole resonance which is spherically symmetric and much too high in energy. On the other hand, the ($E1 : 2p \rightarrow 1s$) and the ($E2 : 3d \rightarrow 1s$) transitions result in excitation of the electric giant dipole and quadrupole resonances, respectively, both of which act as doorway states for fission. Let us consider the specific case of ^{238}U : The giant dipole resonance is located at $E_{GDR} = 12.8\text{MeV}$ and has a width $\Gamma = 6\text{MeV}$ [31]; for the $T = 0$ giant quadrupole resonance the corresponding numbers are $E_{GQR} = 9.9\text{MeV}$ and $\Gamma = 6.8\text{MeV}$ [32]. According to Teller and Weiss [33] and Karpeshin and Nesterenko [2] it is very probable that the $3d \rightarrow 1s$ radiationless transition will be dominant for muon-induced fission, because its transition energy of 9.6MeV is very close to the peak of the giant quadrupole resonance whereas the $2p \rightarrow 1s$ transition energy of 6.6MeV is far off the center of the giant dipole resonance. Experimentally, the situation is controversial: Johansson et al. [22] measured muonic X-rays in coincidence with prompt fission in ^{238}U . From the muonic X-ray intensity ratios for prompt and delayed fission they conclude that $(74 \pm 15)\%$ of all prompt events can be attributed to the $3d \rightarrow 1s$ radiationless transition and only $(26 \pm 15)\%$ to the $2p \rightarrow 1s$ transition. On the other hand, Kaplan et al. [20] find in similar studies a predominance of the E1 transitions in their prompt fission data.

As mentioned in the Introduction, if the nuclear motion is relatively fast (low friction) there is a nonvanishing probability that the muon may be promoted to higher-lying molecular orbitals, e.g. the $2p\sigma$ level from where it may end up attached to the light fission fragment. This gave rise to hopes that the muon attachment probability to the light fragment P_L would depend on the pre-fission scenario. In this case, theoretical studies of the muon-attachment probability to the light fission fragment in combination with experimental data can be utilized to probe the dynamics of prompt fission.

On the other hand, in a series of papers it was pointed out that the fragment motion occurs quasiclassically. The fragment velocity exceeds by ~ 6 times that of the muon in the orbit. Moreover, it satisfies the Massey criterium of adiabaticity which does not promise any significant transition probability.

Fortunately, the presence of the avoided crossing of the $1s\sigma$ and $2p\sigma$ levels favors the transition. As is known, in this case the transition occurs in a narrow vicinity of the crossing. At the same time, the pseudocrossing occurs well beyond the scission point, at a distance which is twice as large as that of the neck rupture for the most

likely pairs of fragments. At this distance, the trajectory of the relative fragment motion $R(t)$ is governed by their mutual Coulomb repulsion. Therefore, knowing the P_L value might only provide us with the instantaneous velocity of the fragments at this point, which could be obtained much more easily from conservation of energy. By contrast, it could be argued that the avoided crossing approaches the point of rupture as the fragment asymmetry increases. This suggests that the P_L value also becomes more sensitive to the pre-fission scenario in this case.

Furthermore, in a series of papers [34, 35] it was noted that the point of rupture itself can be considered as an irregular point where the analyticity of the dependence of $R(t)$ on time is broken. That is rather apparent from the mathematical viewpoint, as the analyticity would assume a unique trajectory in all the domain of its definition, $0 \leq R < \infty$. Actually, the trajectory can be considered unique only after scission, for $R_{sc} < R < \infty$. But before scission, one can provide a rather arbitrary scenario, as we saw when discussing the one- and two-body mechanisms of friction. Moreover, the very position of the scission point itself may be varied within certain limits. We return to this question in a later section.

In fact, the muon appears to be the only available tool for such studies. However, this simple picture is complicated by the fact that transitions to some of the higher-lying levels of the transient muonic molecule (e.g. $2p\pi$ and $2s\sigma$) result again in muon attachment to the heavy fragment.

To obtain an order-of-magnitude estimate for the muon attachment probabilities, we utilize a simple formula derived by Demkov [36] and by Meyerhof [37]. Their model is based on the two lowest molecular levels ($1s\sigma$ and $2p\sigma$) and utilizes first-order perturbation theory to calculate the transition probability from the $1s\sigma$ to the $2p\sigma$ level; within the two-level model, it is equal to the muon attachment probability to the light fission fragment:

$$P_L = \left(1 + e^{2|x|}\right)^{-1}, \quad x = \frac{\pi (I_H - I_L)}{\left(\frac{v}{c}\right) \sqrt{2m_\mu c^2} (\sqrt{I_H} + \sqrt{I_L})}, \quad (3)$$

where I_H and I_L denote the binding energies of the muonic K-shell belonging to the heavy and light fission fragments, respectively, and v is the relative velocity of the fission fragments. For a fragment charge asymmetry $\xi = Z_H/Z_L = 55/39 = 1.41$ (corresponding to the peak of the mass distribution) one finds $I_H = 5.93$ MeV and $I_L = 3.45$ MeV. If we assume that the molecular transition occurs at a relative velocity of the fission fragments of $v = 0.08c$ we obtain a muon attachment probability $P_L = 0.042$ for the light fission fragment; this value decreases to $P_L = 0.015$ if $v = 0.06c$. The choice of the parameters in the Demkov model and its extension are discussed in more detail in the next section.

3 Physical premises

3.1 Analytical properties of the trajectories

The concept of determining the role of the avoided crossing for the transition probability is a milestone in the quasiclassical theory of collisions accompanied with reorganization of the scattering systems, in the case where one or two of the subsystems are described quasiclassically, and the other subsystems are described in terms of quantum mechanics. Most famous are collisions of the Landau-Zener type. Well-known are also the Demkov and Nikitin models.

These models are based on the different character of the energy term's behavior in the vicinity of the scission point. In the two-level approximation, the usual expression for the terms can be written as follows:

$$E_{1,2} = \frac{1}{2}(\epsilon_1 + \epsilon_2) \pm \sqrt{(\epsilon_1 - \epsilon_2)^2 + \Delta^2} . \quad (4)$$

The physical meaning of the parameters ϵ_1, ϵ_2 in eq. (4) is that they are considered to be the non-interacting levels. The parameter Δ describes their interaction, and E_1, E_2 are the true terms, with the interaction taken into account.

The Landau-Zener model deals with intersecting terms ϵ_1, ϵ_2 . The interaction Δ is then considered to be $\Delta = \text{constant}$ in the vicinity of the crossing. In the opposite extreme, the Demkov model considers the case of ϵ_1, ϵ_2 parallel to each other, which is usually the case at large distances. At smaller distances, the terms start to diverge due to the interaction, which is supposed to be of exponential form:

$$\epsilon_1 - \epsilon_2 \equiv \epsilon = \text{constant}, \quad \Delta = \exp(-\lambda R) . \quad (5)$$

The Nikitin model generalizes both the Landau-Zener and Demkov models with the following parameters:

$$\epsilon_1 - \epsilon_2 = \epsilon - B \cos \theta \exp(-\lambda R) , \quad \Delta = B \sin \theta \exp(-\lambda R) . \quad (6)$$

Specifically, the Demkov model is obtained with $\theta = \pi/2$. The level crossing occurs in the complex plane at the point

$$R_c = (\epsilon/B) \exp(i\theta) . \quad (7)$$

Many characteristic features of the muon distribution were consecutively studied within the framework of the Demkov [38, 40] and Nikitin [41] models. The parameters of the models were related to realistic muonic wavefunctions. All the parameters, as well as the relative velocity, entering the expression for the transition probability, have been taken at the point of the avoided crossing. Naturally, pre-fission dynamics was not involved in such an approach, as the pseudocrossing point is beyond the scission point as mentioned in the Introduction. Conclusions

about the pre-fission dynamics could be drawn from comparison with experimental data (e.g., [42]). Moreover, prospects of the study of other manifestations of the fission dynamics, such as muon shake-off due to the neck rupture, have been discussed. These effects are not in the scope of the quasimolecular adiabatic picture considered herein. The results obtained were also applied for the interpretation of many experiments concerning muonic conversion of the prompt fission fragment γ rays, and muon capture by the fragments (e.g., [13] and refs. cited therein).

3.2 The complex trajectory method

What was stated previously about the analytical properties of the trajectory function $R(t)$ can be realized in terms of the complex trajectory method [34, 35, 52].

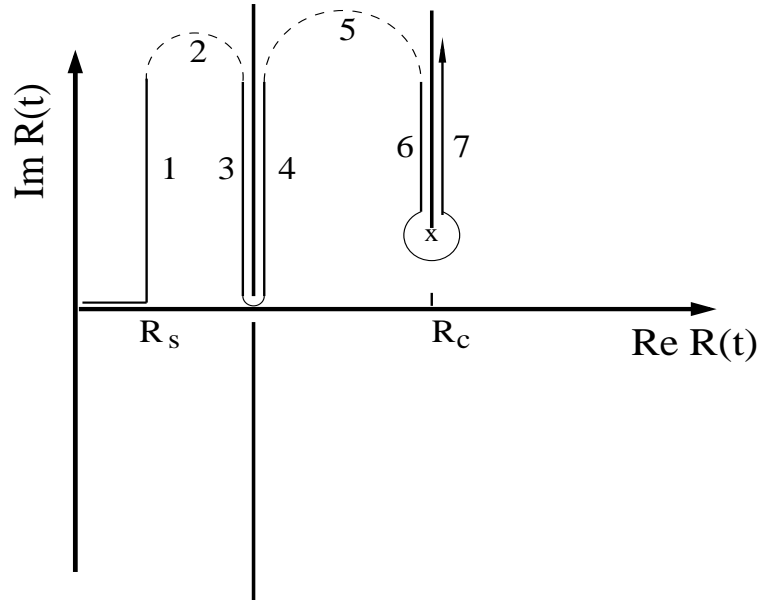


Figure 1: The complex trajectory. The point $R = 0$ corresponds to the united atom limit. The onset of population of the $2p\sigma$ level is at the saddle point R_s . The scission point R_{sc} and the point of avoided crossing R_c are the other singular points, where the integration contour is fixed.

According to this method, the path $R(t)$ corresponding to the trajectory of the relative motion of the fragments from $R = 0$ to $R \rightarrow \infty$ can be deformed and shifted to the upper half-plane of complex R values, with the exception of irregular points.

The reason for such a transformation is that in the upper half-plane the nonadiabatic matrix element vanishes. As a result, the main contribution comes from small segments nearest to the real axis of R , attached to the fixed irregular points. This transformation is shown in Figure 1. The irregular points are, as was mentioned previously, the pseudocrossing point R_c , which is a square-root type branching point, the scission point R_{sc} , and the starting point of the motion which in our case is

reasonable to put on the top of the barrier. Thus, the contributions from the line segments 2 and 5 are expected to vanish for $R \rightarrow \infty$ [47].

We then note that the contributions from the segments 3 and 4 partly cancel one another, being of the opposite sign. Were the scission point a regular point of the trajectory, the cancellation would be complete, and this point would give no contribution to the transition amplitude. This would be the same as the point R_{sc} would be shifted to the upper half-plane, together with the segments 3 and 5. The two vertical cuts in Figure 1 fix the trajectory at the scission point, not allowing one to move it from the real axis of R .

Relative contributions of the scission and pseudocrossing points turn out to be different, depending on the mass split of the fragments. The first contribution is several times smaller than the second one in the case of the most probable mass split. In the case of larger asymmetry, the contribution from scission approximately holds. In contrast, the contribution from the avoided crossing exponentially decreases. For this reason, the attachment probability becomes relatively more sensitive to the pre-fission scenario for more asymmetric fission, though its absolute value decreases. This circumstance was noted in refs. [46, 44], where a higher sensitivity for larger asymmetry was predicted as a consequence of approaching the pseudocrossing point to the prefission area.

We note that in actual calculations, the relative velocity $V(R)$ is smoothly joined at the point R_{sc} from the left and the right, with its derivative. Then the position of R_{sc} is the only parameter which governs the contribution from the scission point. In this schematic picture, the pseudocrossing point appears to be completely independent of the prefission scenario, as the values of integrands along the segments 6 and 7 are determined by analytical continuation of the Coulomb part of the trajectory at $R_{sc} < R < \infty$. This explains why in some papers the resulting transition probability was found not to depend on the precession scenario: as a matter of fact, the position of R_{sc} was not varied in those studies, but only the prefission time t_{sc} [43, 42].

3.3 The Born - Oppenheimer expansion

Many of the first papers devoted to the calculation of the muon distribution were based on the Born - Oppenheimer expansion. We use the following series expansion [6]:

$$\Psi(\mathbf{r}; R(t)) = \sum_n C_n \Phi_n(\mathbf{r}; R(t)) e^{i(\mathbf{p}_n \mathbf{r})} e^{-i \int^t E'_n(t') dt'}. \quad (8)$$

Here $\Psi(\mathbf{r}; R(t))$ is the wavefunction, Φ_n form a full set of quasimolecular wavefunctions. Our basic product functions $\Phi_n(\mathbf{r}; R) e^{i \mathbf{p}_n \mathbf{r}}$ satisfy the time-dependent Schrödinger equation

$$(i \frac{\partial}{\partial t} - H) \Phi_n(\mathbf{r}; R) e^{i \mathbf{p}_n \mathbf{r} - i E'_n t} = 0, \quad (9)$$

with modified eigenvalue $E'_n = E_n + p_n^2/2\mu$, reflecting conservation of energy, and the two-centre Hamiltonian

$$H = -\frac{\Delta}{2\mu} + V_1(|\mathbf{r} - \mathbf{R}_1|) + V_2(|\mathbf{r} - \mathbf{R}_2|). \quad (10)$$

When the internuclear distance $R \rightarrow \infty$ each of the functions Φ_n correlates with a certain muonic state n of the corresponding fragment.

The momentum-translation exponents (m.t.e.) are introduced in eq. (8), where $\mathbf{p}_n = \mu\mathbf{v}_n$, with μ the muon mass, and v_n a constant, equal to the velocity of the fragment in the asymptotic region. This condition is not essential, and can be easily abandoned [34]. On the other hand, the orthogonality of the basis functions is broken in this description.

Substituting the expansion (1) into the time-dependent Schrödinger equation, and neglecting small non-orthogonal terms, we get the following set of coupled equations

$$\frac{dC_i}{dR} = - \sum_k F_{ik} C_k, \quad (11)$$

$$F_{ik} = \mathcal{M}_{ik} e^{-i \int^R [(E'_k - E'_i(R'))/V(R')] dR'}, \quad (12)$$

$$\mathcal{M}_{ik} = \langle \Phi_i e^{i(\mathbf{p}_i \mathbf{r})} | \frac{\partial}{\partial R} - \frac{\mathbf{v}_i + \mathbf{v}_k}{2V(R)} \nabla | \Phi_k e^{i(\mathbf{p}_k \mathbf{r})} \rangle, \quad (13)$$

where the differential operators act only on the wavefunctions Φ_i or Φ_k , and $V(R)$ stands for the relative velocity of the fragments.

The equations are to be solved with the initial condition

$$C_i = \delta_{i1} \quad \text{for } R = R_i, \quad (14)$$

denoting that the muon is in the ground state at the starting point R_i .

Note, that for $R \rightarrow \infty$, the modified basis regains its primordial orthogonality, as p_i are the same for each state i on one fragment. Therefore, the amplitudes of decomposition over the modified basis acquire the usual physical meaning. These amplitudes must be used for the determination of physical probabilities, rather than the amplitudes in the traditional basis without the m.t.e.

Incorporation of the m.t.e. thus modifies the non-adiabatic matrix element from

$$\mathcal{M}' = \frac{\partial}{\partial R} \quad (15)$$

to

$$\mathcal{M}'' = \frac{\partial}{\partial R} + \frac{v_1 - v_2}{2V(R)} \frac{\partial}{\partial z}, \quad (16)$$

according to eq. (13) with the momenta $p_n = \text{const.}$

Equation (10) poses a two-dimensional eigenvalue problem. It has been solved numerically in ref.[42] by making use of the finite element method. On the other hand, it should be noted that using in eq. (8) the asymptotic values of $p_n = const$ is only justified in the limit $R \rightarrow \infty$. For small R , where the relative velocity of the fragments is several times smaller, the perturbation brought by the second terms in eqs. (13), (16) to the non-adiabatic transition operator is in principle excessively large. This difficulty was successfully overcome [34].

The problem (10) has been solved in spheroidal coordinates

$$\psi, \eta = (r_1 \pm r_2)R \quad (17)$$

$$1 \leq \psi < \infty, \quad -1 \leq \eta \leq 1 \quad . \quad (18)$$

It is noteworthy that recently, spheroidal coordinates were also applied in refs. [48, 49], where the dynamics was studied of light charged particle emission in spontaneous cold fission of ^{252}Cf . In these coordinates, the Laplacian becomes

$$\Delta_{\psi, \eta} = \frac{4}{R^2(\psi^2 - \eta^2)} \left[\frac{\partial}{\partial \psi} (\psi^2 - 1) \frac{\partial}{\partial \psi} + \frac{\partial}{\partial \eta} (1 - \eta^2) \frac{\partial}{\partial \eta} \right] \quad . \quad (19)$$

A finite-differences method on a rectangular grid (18) is used to obtain a first approximation to the solution of the problem (10), generally a rather poor one. The final solution of the problem is found by minimization of the Rayleigh-Ritz functional of the problem (10):

$$\mathcal{R}(\Phi) = \frac{\int \int_G [\mathcal{T}(\Phi) + \rho(\psi, \eta) (V_1 + V_2) \Phi^2] d\psi d\eta}{\int \int_G \rho(\psi, \eta) \Phi^2 d\psi d\eta} \quad , \quad (20)$$

where

$$\mathcal{T}(\Phi) = \frac{R}{4} [(\psi^2 - 1) \left(\frac{\partial \Phi}{\partial \psi} \right)^2 + (1 - \eta^2) \left(\frac{\partial \Phi}{\partial \eta} \right)^2] \quad , \quad (21)$$

and

$$\rho(\psi, \eta) = \frac{R^3}{8} (\psi^2 - \eta^2) \quad . \quad (22)$$

The minimization is achieved by the finite-element method. For realization of the method, all the area G of variables (18) is devided into N rectangular pieces g^j . Within each element, a biquadratic function is defined as follows:

$$\phi_j(\psi, \eta) = a_0^j + a_1^j \psi + a_2^j \eta + a_3^j \psi \eta + a_4^j \psi^2 + a_5^j \eta^2 + a_6^j \psi^2 \eta + a_7^j \psi \eta^2 \quad . \quad (23)$$

In the basis of functions ϕ_j , $j = 1, \dots, N$, the problem (20) is reduced to a generalized algebraic eigenvalue problem $K\Phi = EM\Phi$, with the “stiffness” matrix K , and M the matrix of “mass”. The problem is then solved by the inverse iteration method [50].

Many results concerning the influence of the fission dynamics on the muon attachment probabilities were obtained by direct numerical integration of the time-dependent Schrödinger and Dirac equations on a 3-dimensional grid. This method and the results obtained are presented in the next sections.

4 Theoretical Developments

Because the nuclear excitation energy in muon-induced fission exceeds the fission barrier height it is justified to treat the fission dynamics classically (no barrier tunneling). For simplicity, we describe the fission path by one collective coordinate R ; the classical collective nuclear energy has the form

$$E_{\text{nuc}} = \frac{1}{2}B(R)\dot{R}^2 + V_{\text{fis}}(R) + E_{\mu}(R). \quad (24)$$

We utilize a coordinate dependent mass parameter $B(R)$ [4] and an empirical double-humped fission potential $V_{\text{fis}}(R)$ [53] which is smoothly joined with the Coulomb potential of the fission fragments at large R . The last term in Eq. (24) denotes the instantaneous muonic binding energy which depends on the fission coordinate; this term will be defined later.

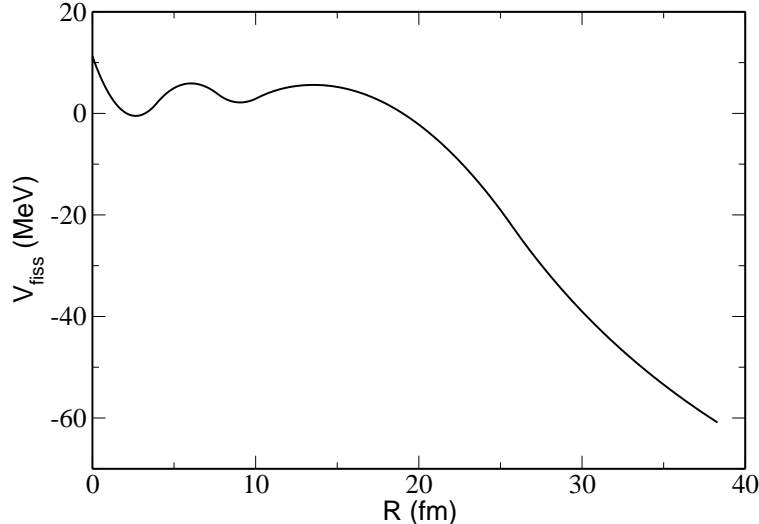


Figure 2: Phenomenological fission potential for $^{237}_{93}Np$, for a mass asymmetry parameter $A_H/A_L = 1.40$. The potential is constructed from four parabolic sections and is smoothly joined with the Coulomb potential of the fission fragments at large distance R .

To account for the nuclear energy dissipation between the outer fission barrier and the scission point, we introduce a friction force which depends linearly on the velocity. In this case, the dissipation function D is a simple quadratic form in the velocity

$$\dot{E}_{\text{nuc}}(t) = -2D = -f\dot{R}^2(t). \quad (25)$$

The adjustable friction parameter f determines the dissipated energy; it is the only unknown quantity in the theory.

For the dynamical description of the muonic wavefunction during prompt fission, the electromagnetic coupling between muon and nucleus ($-e\gamma_\mu A^\mu$) is dominant; the weak interaction is negligible. Because of the nonrelativistic motion of the fission fragments the electromagnetic interaction is dominated by the Coulomb interaction

$$A^0(\mathbf{r}, t) = \int d^3 r' \frac{\rho_{\text{nuc}}(\mathbf{r}', t)}{|\mathbf{r} - \mathbf{r}'|}. \quad (26)$$

The muonic binding energy in the ground state of an actinide muonic atom amounts to 12 percent of the muonic rest mass; hence non-relativistic calculations, while qualitatively correct, are limited in accuracy. Several theory groups have demonstrated the feasibility of such calculations [9, 12, 13] which are based on the time-dependent Schrödinger equation

$$[-\frac{\hbar^2}{2m} \nabla^2 - eA^0(\mathbf{r}, t)] \psi(\mathbf{r}, t) = i\hbar \frac{\partial}{\partial t} \psi(\mathbf{r}, t). \quad (27)$$

In 1992, Oberacker et al.[14, 4] developed a numerical algorithm to solve the relativistic Dirac problem on a three-dimensional Cartesian lattice. The time-dependent Dirac equation for the muonic spinor wave function in the Coulomb field of the fissioning nucleus has the form

$$H_D(t) \psi(\mathbf{r}, t) = i\hbar \frac{\partial}{\partial t} \psi(\mathbf{r}, t), \quad (28)$$

where the Dirac Hamiltonian is given by

$$H_D(t) = -i\hbar c \alpha \cdot \nabla + \beta mc^2 - eA^0(\mathbf{r}, t). \quad (29)$$

Our main task is the solution of the Dirac equation for the muon in the presence of a time-dependent external Coulomb field $A^0(\mathbf{r}, t)$ which is generated by the fission fragments in motion. Note the coupling between the fission dynamics, Eq. (24), and the muon dynamics, Eq. (28), via the instantaneous muonic binding energy

$$E_\mu(R(t)) = \langle \psi(\mathbf{r}, t) | H_D(t) | \psi(\mathbf{r}, t) \rangle \quad (30)$$

which depends on the fission coordinate; the presence of this term increases the effective fission barrier height.

5 Lattice Representation: Basis-Spline Expansion

For the numerical solution of the time-dependent Dirac equation (28) it is convenient to introduce dimensionless space and time coordinates

$$\mathbf{x} = \mathbf{r}/\lambda_c \quad \lambda_c = \hbar/(m_\mu c) = 1.87 \text{ fm}$$

$$\tau = t/\tau_c \quad \tau_c = \lambda_c/c = 6.23 \times 10^{-24} s \quad (31)$$

where λ_c denotes the reduced Compton wavelength of the muon and τ_c the reduced Compton time. For the lattice representation of the Dirac Hamiltonian and spinor wave functions we introduce a 3-dimensional rectangular box with a uniform lattice spacing Δx . The lattice points are labeled $(x_\alpha, y_\beta, z_\gamma)$.

Our numerical algorithm is the Basis-Spline collocation method [57]. Basis-Spline functions $B_i^M(x)$ are piecewise-continuous polynomials of order $(M - 1)$. These may be thought of as generalizations of the well-known “finite elements” which are B-Splines with $M = 2$.

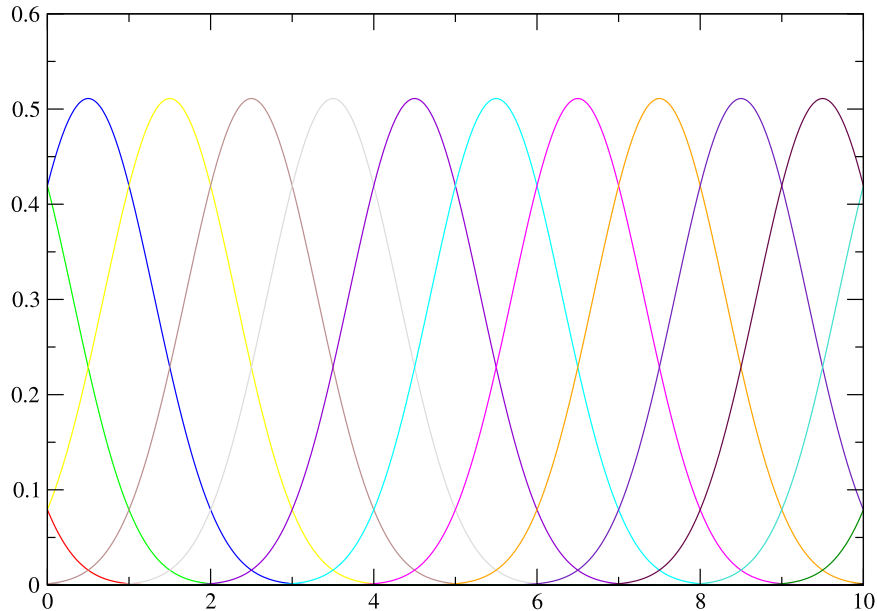


Figure 3: Set of Basis Splines of order $M = 5$ using periodic boundary conditions.

There exists an extensive literature on Basis-Spline theory, developed by mathematicians [56]. In 1991, Umar et al.[57] applied the method to the numerical solution of problems in atomic and nuclear physics on a lattice; this paper discusses the B-Spline collocation method, periodic and fixed boundary conditions, the solution of various 1-D radial problems (Schrödinger, Poisson and Helmholtz equations), and the solution of 3-D Cartesian problems (Poisson equation). In a later paper in 1991, Umar et al. solved the nuclear static and time-dependent Hartree-Fock equations

on a 3-D lattice [58]. During 1992-1995, Oberacker et al.[14, 4] and Wells et al.[59] applied the B-Spline collocation method to the static and time-dependent Dirac equation which overcame the “fermion doubling problem” which one encounters with the finite-difference method. Very recently, we have used both the B-Spline collocation and Galerkin methods for the solution of the Hartree-Fock-Bogoliubov nuclear structure problem [60, 61].

To illustrate the B-Spline collocation method let us consider a wave function which depends on one space coordinate x ; we represent the wave function on a finite spatial interval as a linear superposition of B-Spline functions

$$\psi(x_\alpha) = \sum_{i=1}^N B_i^M(x_\alpha) c^i. \quad (32)$$

In the Basis-Spline collocation method, local operators such as the EM potential A^0 in Eq. (29) become diagonal matrices of their values at the grid points (collocation points), i.e. $V(x) \rightarrow V_\alpha = V(x_\alpha)$. The matrix representation of derivative operators is more involved [59]. For example, the first-derivative operator of the Dirac equation has the following matrix representation on the lattice

$$D_\alpha^\beta \equiv \sum_{i=1}^N B'_{\alpha i} B^{i\beta}, \quad (33)$$

where $B'_{\alpha i} = [dB_i^M(x)/dx]|_{x=x_\alpha}$. Furthermore, we use the shorthand notation $B_{\beta i} = B_i^M(x_\beta)$ for the B-spline function evaluated at the collocation point x_β , and the inverse of this matrix is denoted by $B^{i\beta} = [B^{-1}]_{\beta i}$. Because of the presence of this inverse, the operator D_α^β will have a nonsparse matrix representation. In the present calculations we employ B-Splines of order $M = 5$. Eq. (32) can readily be generalized to three space dimensions; in this case the four Dirac spinor components $\psi^{(p)}$, $p = (1, \dots, 4)$ are expanded in terms of a product of Basis-Spline functions

$$\psi^{(p)}(x_\alpha, y_\beta, z_\gamma, t) = \sum_{i,j,k} B_i^M(x_\alpha) B_j^M(y_\beta) B_k^M(z_\gamma) c_{(p)}^{ijk}(t), \quad (34)$$

i.e. the lattice representation of the spinor wave function is a vector with $N = 4 * N_x * N_y * N_z$ complex components. Hence, it is impossible to store H_D in memory because this would require the storage of N^2 complex double-precision numbers. We must therefore resort to iterative methods for the solution of the matrix equation which do not require the storage of H_D .

We solve the time-dependent Dirac equation in two steps: first, we consider the static Coulomb problem at time $t = 0$, i.e. the muon bound to an actinide nucleus

$$H_D(t = 0)\psi_{\text{gs}} = E_{\text{gs}}\psi_{\text{gs}}. \quad (35)$$

This static problem is solved by an iterative procedure (damped relaxation method [4, 59]). The second part of our numerical procedure is the solution of the time-dependent Dirac equation (28) by a Taylor-expansion of the propagator. For an infinitesimal time step Δt we find

$$\psi(t + \Delta t) = U(t + \Delta t, t)\psi(t) \approx (1 + \sum_{n=1}^N \frac{(-iH\Delta t)^n}{n!})\psi(t). \quad (36)$$

We have thus reduced the original problem to a series of (matrix) \times (vector) operations which can be executed with high efficiency on vector or parallel supercomputers without explicitly storing the matrix in memory.

6 Discussion of Numerical Results

In the following we present results for prompt fission of $^{237}_{93}\text{Np}$ induced by the $E2 : (3d \rightarrow 1s, 9.5\text{MeV})$ muonic transition. All results reported here are for a 3-D Cartesian lattice of size $L_x = L_y = 67 \text{ fm}$ and $L_z = 146 \text{ fm}$ with $N_x * N_y * N_z = 25 * 25 * 53$ lattice points with a uniform lattice spacing $\Delta x = 1.5\lambda_c = 2.8\text{fm}$. Depending on the value of the friction coefficient, we utilize between 1,200 – 1,900 time steps with a step size $\Delta t = 1.5\tau_c = 9.3 \times 10^{-24} \text{ s}$. The computer source code is written in Fortran 95. Typical production runs use 25 MB of memory and require 5.3 hours of CPU time on an Intel Pentium-4 (1.7GHz) GNU/LINUX workstation. The same job takes 3.2 CPU hours on an IBM-SP2 supercomputer at NERSC (serial run on one processor).

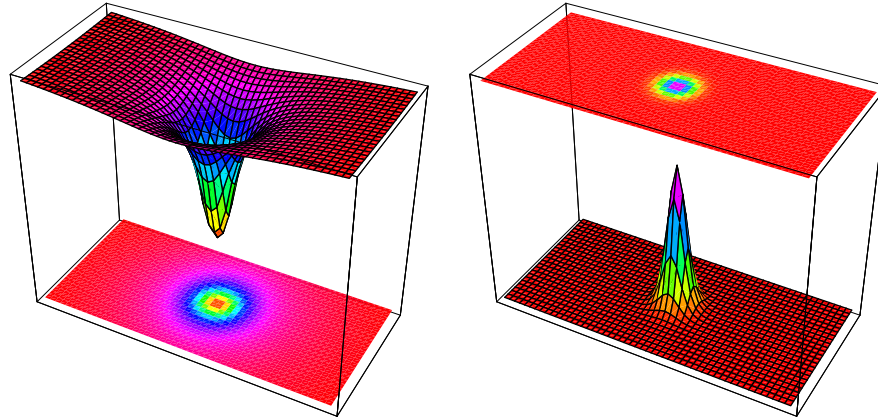


Figure 4: Prompt muon-induced fission of $^{237}_{93}\text{Np}$ for a fission fragment mass asymmetry $\xi = A_H/A_L = 1.10$ at $E^* = 9.5 \text{ MeV}$. Shown is the Coulomb interaction energy between the muon and the fissioning nucleus (left) and the corresponding muon position probability density (right) at time $t = 0$ during fission. Zero friction ($f = 0$) has been assumed.

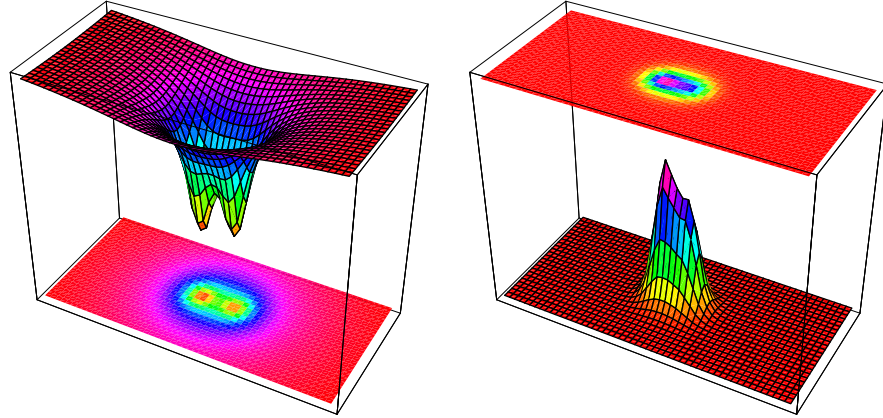


Figure 5: Same as Fig.4, except at time step $t = 6.5 \times 10^{-21}$ s.

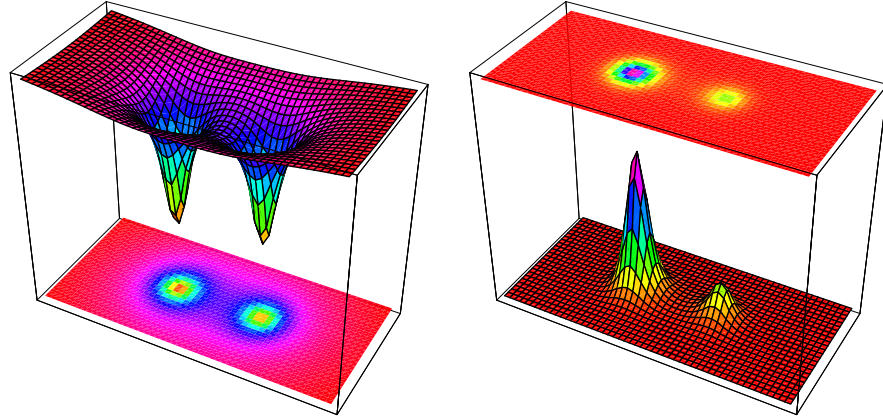


Figure 6: Same as Fig.4, except at time step $t = 8.4 \times 10^{-21}$ s.

Fig. 4 shows the Coulomb interaction energy between the muon and the neptunium nucleus (left) and the corresponding muon position probability density (right) at time $t = 0$ during fission. At this moment, the actinide nucleus is situated in its deformed ground state minimum with quadrupole deformation $\beta_2 = 0.27$. Figures 5,6,7 show the time-development of the Coulomb interaction and the corresponding muon position probability density during fission. The calculation has been done for an asymptotic fragment mass asymmetry $\xi = A_H/A_L = 1.10$. In the last two time steps the Coulomb potential wells of the two separated fission fragments are clearly visible; the deeper well on the left is generated by the heavier fission fragment. We observe a clear spatial correlation between the positions of the potential minima and the muon probability density maxima. As expected, the muon sticks predomi-

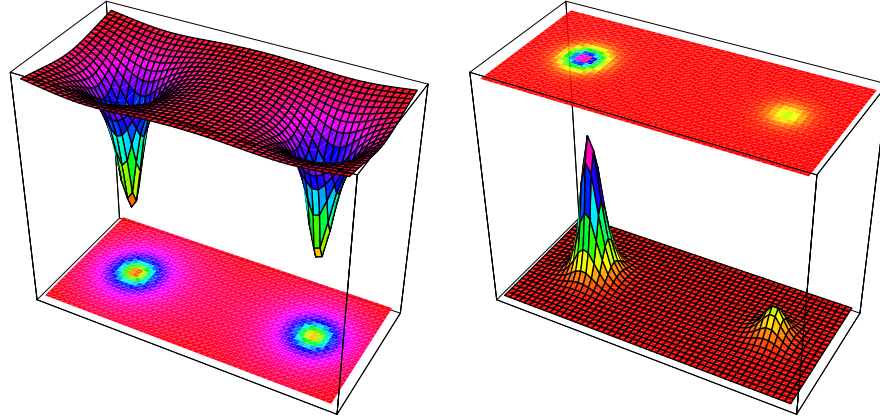


Figure 7: Same as Fig.4, except at time step $t = 1.1 \times 10^{-20}$ s.

nantly to the heavy fragment (large bump on the left in Fig.7), but since the mass asymmetry in this case is very small ($\xi = A_H/A_L = 1.10$) the muon attachment to the light fission fragment (bump on the right) is relatively large. By integrating the muon probability densities associated with the heavy and light fission fragments at large internuclear distances, we can infer the muon attachment probabilities to the heavy and light fragments, P_H and P_L , respectively. From Fig.7 we find $P_L = 0.20$.

One might ask whether the muon will always remain bound during fission; what is the probability for ionization? To investigate this question we have plotted the muon position probability density on a logarithmic scale.

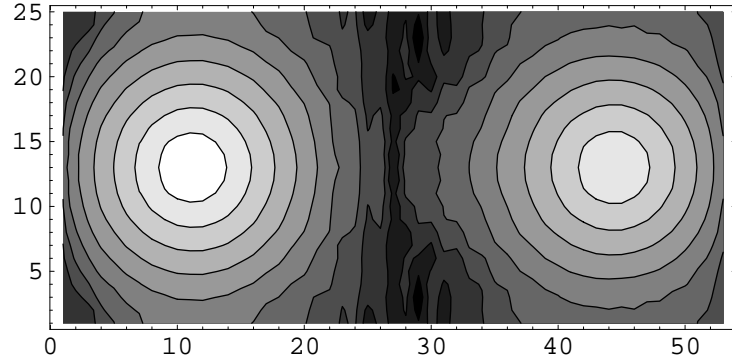


Figure 8: Contour plot of the logarithm of the muon probability density at $t = 1.1 \times 10^{-20}$ s shows no evidence of muon ionization.

In coordinate space, any appreciable muon ionization would show up as a “probability cloud” that is separating from the fission fragments and moving towards the boundaries of the lattice. Fig. 8 shows no evidence for such an event in our numer-

ical calculations. Hence, we conclude that the probability for muon ionization P_{ion} is substantially smaller than the muon attachment probability to the light fission fragment which is always clearly visible in our logarithmic plots, even at large mass asymmetry. From this we estimate that $P_{\text{ion}} < 10^{-4}$.

As in all lattice calculations, we need to demonstrate convergence of our results in terms of the lattice size and lattice spacing. Fig. 9 shows the asymptotic muon attachment probability P_L as a function of the total number of lattice points. In all of our production runs we use a lattice with a total of $N_x * N_y * N_z = 25 * 25 * 53 = 33,125$ lattice points. It is apparent that the muon attachment probabilities (and other related observables) have indeed converged.

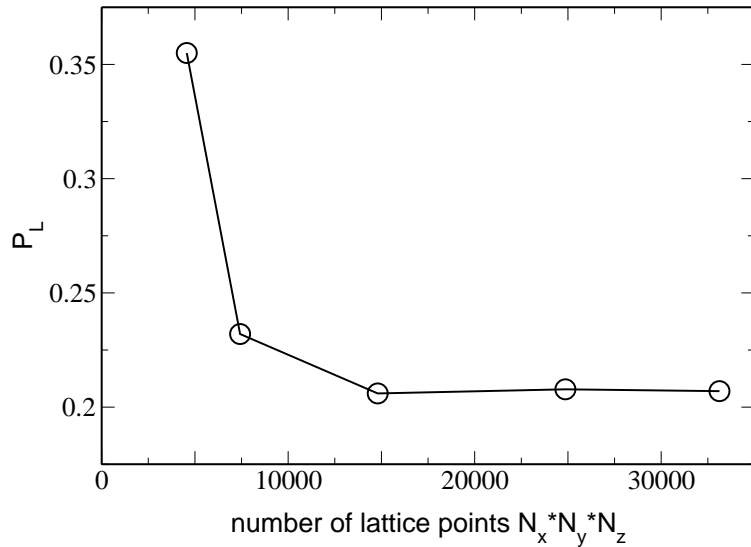


Figure 9: Demonstration of numerical convergence of muon attachment probability for $^{237}_{93}\text{Np}$. Calculations use a mass asymmetry of 1.10 and zero friction.

Fig. 10 shows that P_L depends strongly on the fission fragment mass asymmetry. This is easily understood: for equal fragments we must have $P_L = 0.5$, and for large mass asymmetry it is energetically favorable for the muon to be bound to the heavy fragment, hence P_L will be small.

Fig. 11 shows the nuclear energy dissipation (in form of neutron- and γ -emission) as a function of time; in our model, friction is confined to the region between the outer fission barrier and the scission point; for friction parameters $f = 200$ and $f = 500$, we obtain total dissipated energies $E_{\text{diss}} = 14.2\text{MeV}$ and 22.0MeV , respectively.

In Fig. 12 we examine the dependence of P_L on the dissipated nuclear energy, E_{diss} , during fission. In our model, friction takes place between the outer fission barrier and the scission point. When the dissipated energy is computed from equa-

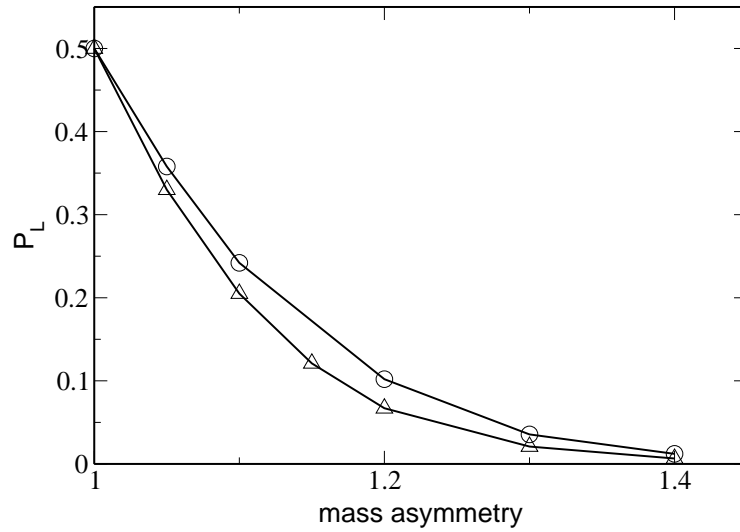


Figure 10: Muon attachment to light fission fragment vs. fission fragment mass asymmetry. upper curve: $^{238}_{92}\text{U}$, lower curve: $^{237}_{93}\text{Np}$. The calculations assume zero friction.

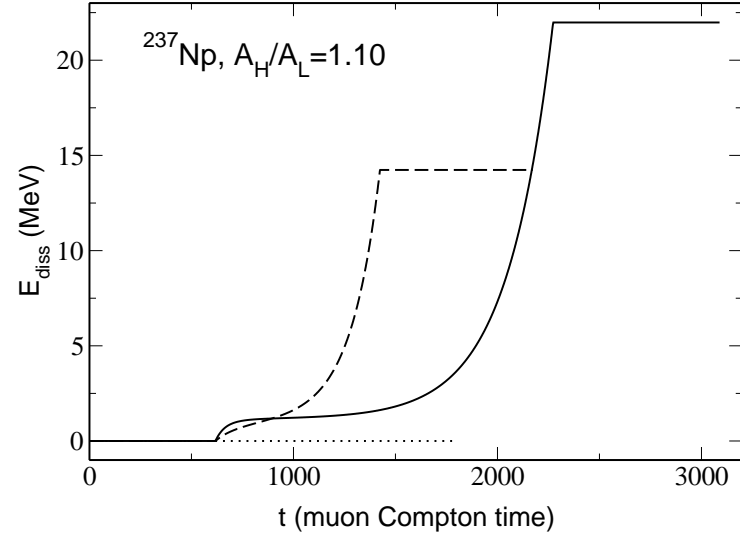


Figure 11: Energy dissipated during fission, for friction parameters $f = 0$, $f = 200$ and $f = 500$.

tion (25) we find an almost linear dependence of the muon attachment probability

on E_{diss} ; unfortunately, this dependence is rather weak.

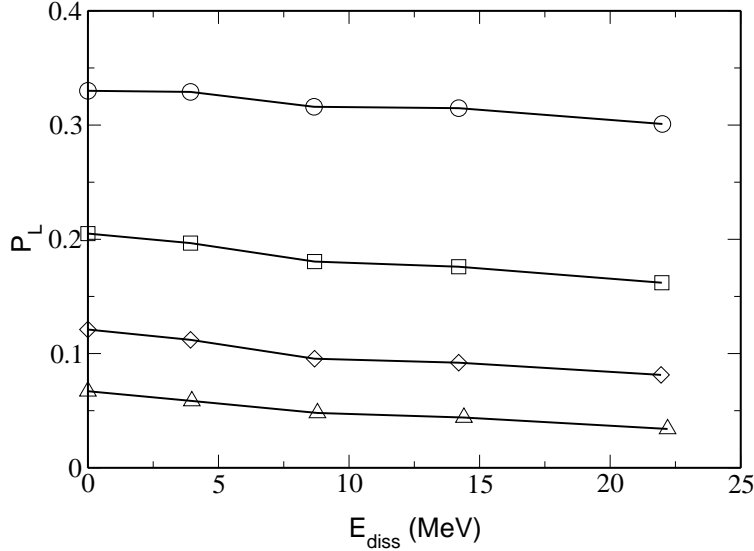


Figure 12: Muon attachment probability to the light fission fragment as function of nuclear energy dissipation for ^{237}Np . Results are shown for fragment mass asymmetries $\xi = 1.05$ (upper curve), 1.10, 1.15, and 1.20 (lower curve).

We would like to point out that the theoretical values for P_L obtained in this work are smaller than those reported in our early calculations [14, 4]. There are two reasons for this: (a) the size of the lattice and (b) the lattice representation of the first derivative operator in the Dirac equation. Because of constraints in the amount of computer time available to us we utilized a smaller cubic lattice in our prior calculations [4] with $N_x * N_y * N_z = 29^3$ lattice points. In recent years, we were able to increase the size of the lattice substantially, in particular in fission (z -) direction (see Fig. 9). Regarding the lattice representation of the first derivative operator, Eq. (33), in the Dirac equation: in ref. [14, 4] we utilized a combination of forward and backward derivatives for the upper and lower spinor wave function components; after extensive testing of Coulomb potential model problems with known analytical solutions we have found that the symmetric derivative operator provides a more faithful lattice representation. The results reported here and in ref. [15] have been obtained utilizing the symmetric derivative prescription.

7 Comparison of Theory with Experiment

Prompt muon-induced fission was first observed experimentally by Diaz et al. [62]. More recent experiments by Ahmad et al. [19] yield a total fission probability per

muon stop $P_f = 0.068$ for ^{238}U and a ratio $P_f(\text{prompt})/P_f(\text{delayed}) = 0.089$.

There are only few experimental data on muon attachment available for comparison with our theory. Schröder *et al.* [18] measured for the first time mean lifetimes of muons bound to fission fragments of several actinide nuclei. The muon decays from the K-shell of the muonic atom through various weak interaction processes at a characteristic rate $\lambda = \lambda_0 + \lambda_c$, where $\lambda_0 = (2.2 \times 10^{-6} \text{ s})^{-1}$ is the free leptonic decay rate for the decay process $\mu^- \rightarrow e^- + \bar{\nu}_e + \nu_\mu$ and λ_c denotes the nuclear capture rate; λ_c depends upon the charge and mass of the fission fragment. From the observed lifetime $\tau_\mu = 1.30 \times 10^{-7} \text{ s}$ Schröder *et al.* estimated an upper limit for the muon attachment probability $P_L \leq 0.1$. It must be emphasized that this number represents an integral over the whole fission mass distribution and, hence, cannot be directly compared to the numbers given in Fig. 12.

The most complete experiments have been carried out by Rissee *et al.* [25] using the muon beam of the $\pi E3$ channel at the Paul Scherrer Institute (PSI) in Switzerland. For this purpose, a fission chamber has been inserted into the electron spectrometer SINDRUM I. The incident muons are detected by a scintillation counter. An event is defined by a $(\mu^-, f_1 f_2 e^-)$ coincidence where the fission fragments are observed in prompt and the muon decay electrons in delayed coincidence with respect to the incident muon. The magnetic field of the electron spectrometer allows for a reconstruction of the electron trajectories. Thus, it is possible to determine whether the muon decay electrons originate from the heavy or the light fission fragment.

For several mass bins of the light fission fragment, muon attachment probabilities P_L have been measured; the experimental data are given in Table 1. It should be emphasized that the mass bins are relatively broad. Because the theoretical values for P_L depend strongly on the mass asymmetry it is not justified to assume that P_L remains constant within each experimental mass bin. Instead, to allow for a comparison between theory and experiment, we have to multiply the theoretical P_L values in Fig. 12 with a weighting factor that accounts for the measured relative mass distribution [25] of the prompt fission events within this mass bin. We subsequently integrate the results over the sizes of the experimental mass bins. Due to the relatively low excitation energy in muon-induced fission, the fission mass distribution exhibits a maximum at $\xi = A_H/A_L = 1.4$ and falls off rather steeply for values larger or smaller than the maximum. This means that the large values of $P_L \approx 0.5$ at or near fission fragment symmetry $\xi = 1.0$ will be strongly suppressed. The resulting theoretical values for P_L are given in the last column of Table 1. It is apparent that our theory agrees rather well with experiment. Because of the size of the error bars in the experiment and because of the weak dependence of the theoretical values of P_L on the dissipated energy, it is not possible to extract very precise information about the amount of energy dissipation.

From a comparison of our theoretical result for the mass bin $A_L = 118.5 \rightarrow 111.5$ with the measured data we extract a dissipated energy of order 10 MeV for ^{237}Np

Table 1: Muon-attachment probabilities to the light fission fragment, P_L , for $^{237}\text{Np}(\mu^-, f)$. Exp. data are taken from ref.[25].

mass bin A_L	mass asymmetry	$P_L(\text{exp})$	$P_L(\text{theo})$
$118.5 \rightarrow 111.5$	$1.000 \rightarrow 1.126$	$(25.5 \pm 8.5) \times 10^{-2}$	$26.0 \times 10^{-2}, E_{\text{diss}} = 0\text{MeV}$ $22.3 \times 10^{-2}, E_{\text{diss}} = 22\text{MeV}$
$111.5 \rightarrow 104.5$	$1.126 \rightarrow 1.268$	$(9.7 \pm 2.6) \times 10^{-2}$	$6.62 \times 10^{-2}, E_{\text{diss}} = 0\text{MeV}$ $3.51 \times 10^{-2}, E_{\text{diss}} = 22\text{MeV}$

while the second mass bin $A_L = 111.5 \rightarrow 104.5$ is more compatible with zero dissipation energy. We like to point out that the value $E_{\text{diss}} = 10$ MeV agrees with results from other low-energy fission measurements that are based on the odd-even effect in the charge yields of fission fragments [65]. In addition to ^{237}Np we have also studied muon-induced fission of ^{238}U ; the results for muon attachment are very similar (see Fig. 10).

8 Outlook: calculation of dissipation in fission

By making use of the commutators $[\frac{\partial}{\partial R}, H]$, $[\frac{\partial}{\partial R}, z]$ one can express the non-adiabatic matrix elements (16) in terms of the mean-field derivatives and the energy differences of the initial and final energies:

$$\mathcal{M}''_{ik} = \frac{1}{\Delta E_{ik}} \left(\frac{d}{dR} + \frac{v_1 - v_2}{2V(R)} \frac{\partial}{\partial z} \right) V(\vec{r}) . \quad (37)$$

$V(\vec{r})$ in eq. (37) is the mean field potential. In the two-center model it can be written as follows:

$$V(\vec{r}) = \begin{cases} V_1(|\vec{r} - \vec{R}_1|) & \text{for } z < 0 \\ V_2(|\vec{r} - \vec{R}_2|) & \text{for } z \geq 0 \end{cases} \quad (38)$$

As the derivative is essentially non-zero at the nuclear surface, this is in the spirit of the well-known semi-classical wall-and-window model, where dissipation arises from the interaction with the walls of a fissile nucleus.

We note that the change of the mean potential (38) during separation of the fragments is due to two reasons: One is the change of the potential due to its radial

dependence through $V_i(|\vec{r} - \vec{R}_i|)$. The corresponding contribution to the matrix element (37) cancels [6] due to the equality

$$\frac{\partial}{\partial R} + \frac{\partial}{\partial z} \equiv 0 , \quad (39)$$

which can be obtained by direct calculation.

The other contribution is due to “breathing” of each of the nascent fragments, which arises from the change of its nuclear radius R_0 :

$$\frac{\partial}{\partial R_i} V_i(|\vec{r} - \vec{R}_i|) = \frac{\partial V_i(|\vec{r} - \vec{R}_i|)}{\partial R_0} \frac{\partial R_0}{\partial R} . \quad (40)$$

In the form (40), the perturbation Hamiltonian was applied for calculating the energy dissipated during saddle to scission descent [6] within the two-center harmonic oscillator model. The calculated amount turns out to be rather small (about 1 MeV) which gives evidence for a rather undamped motion for this kind of friction. The result is in agreement with what was said in the Introduction about this mechanism of nuclear friction. It also agrees with the conclusion drawn from comparison of the calculated muon attachment probabilities with experiment.

9 Conclusions

In this paper, we study the process of prompt muon-induced fission of actinide nuclei. The nuclei are excited by radiationless transitions (inverse internal conversion). For example, in $^{238}_{92}\text{U}$ the $E1 : (2p \rightarrow 1s)$ and the $E2 : (3d \rightarrow 1s)$ muonic transitions result in excitation of the nuclear giant dipole and giant quadrupole resonances, respectively, which act as doorway states for fission. It is very probable that the $(3d \rightarrow 1s, 9.5\text{MeV})$ transition in the muonic atom will be dominant for muon-induced fission, because the transition energy is very close to the peak of the $T = 0$ giant quadrupole resonance of the nucleus ($E_{GQR} = 9.9\text{MeV}$). By contrast, there is a mismatch between the $(2p \rightarrow 1s, 6.6\text{MeV})$ muonic transition energy and the center of the giant dipole resonance which is located at $E_{GDR} = 12.8\text{MeV}$. Because the muon lifetime is long compared to the timescale of prompt nuclear fission, the motion of the muon in the Coulomb field of the fissioning nucleus may be utilized to learn about the dynamics of fission.

We have studied the dynamics of a muon bound to a fissioning actinide nucleus in two different ways: first, using the non-relativistic time-dependent Schrödinger equation, the Born-Oppenheimer expansion method was utilized. This method relies on a set of quasimolecular wavefunctions, and the fission dynamics is described classically.

In the second method, we have solved the relativistic time-dependent Dirac equation on a 3-D Cartesian lattice using Basis-Spline expansion techniques. (The 3-D lattice makes it possible to investigate nuclear fission shapes that are not axially

symmetric. However, in the present study we always assume axial nuclear symmetry, for simplicity). The principal advantage of the coordinate lattice method is that it does not depend on the validity of an “atomic” or “molecular” wavefunction basis set. Furthermore, the method accounts not only for transitions between bound muonic states, but is also describes the possible ionization of the muon during fission: in coordinate space, any appreciable muon ionization would show up as a “probability cloud” that is separating from the fission fragments and moving towards the boundaries of the lattice. Fig. 8 shows no evidence for such an event in our numerical calculations.

Our time-dependent Dirac equation calculations predict a strong mass asymmetry dependence of the muon attachment probability P_L to the light fission fragment; this feature is in agreement with experimental data. The theory also predicts a (relatively weak) dependence of P_L on the dissipated energy. By comparing our theoretical results to the experimental data of ref. [25] we extract a dissipated energy of order $0 - 10$ MeV for ^{237}Np (see Table 1). Using the dissipation function defined in Eq. (25), the 10 MeV value corresponds to a fission time delay from saddle to scission of order 2×10^{-21} s.

Acknowledgements

This work has been partially supported by the U.S. Department of Energy under grant No. DE-FG02-96ER40963 with Vanderbilt University. Some of the numerical calculations were carried out with the IBM-RS/6000 SP supercomputer (“Seaborg”) at the National Energy Research Scientific Computing Center which is supported by the Office of Science of the U.S. Department of Energy.

References

- [1] Y.N. Kim, *Mesic Atoms and Nuclear Structure*, (North-Holland, Amsterdam, 1971).
- [2] F.F.Karpeshin and V.O.Nesterenko. J. Phys. **G17**, 705 (1991); JINR report No. E4-82-694, Dubna, 1982.
- [3] R.W. Hasse, Rep. Prog. Phys. **41**, 1027 (1978).
- [4] V.E. Oberacker, A.S. Umar, J.C. Wells, C. Bottcher, M.R. Strayer and J.A. Maruhn, *Phys. Rev. C* **48** (1993) 1297.
- [5] K.T.R. Davies, A.J. Sierk and J.R. Nix, *Phys. Rev. C* **13** (1976) 2385.
- [6] F.F.Karpeshin. *Yad. Fiz.*, **63**, 799 (2000). (*English transl. Physics of Atomic Nuclei (USA)*, **63**, 729 (2000))

- [7] A. Gavron, A. Gayer, J. Boissevain, H.C. Britt, T. C. Awes, J. R. Beene, B. Cheynis, D. Drain, R. L. Ferguson, F. E. Obenshain, F. Plasil, G. R. Young, G. A. Petitt and C. Butler, *Phys. Rev. C* **35**, 579 (1987).
- [8] D.J. Hofmann *et al.*, *Phys. Rev. C* **51** (1995) 2597.
- [9] J.A. Maruhn, V.E. Oberacker and V. Maruhn-Rezwani, *Phys. Rev. Lett.* **44**, 1576 (1980).
- [10] Z.Y. Ma, X.Z. Wu, G.S. Zhang, Y.C. Cho, Y.S. Wang, J.H. Chiou, S.T. Sen, F.C. Yang and J.O. Rasmussen, *Nucl. Phys. A* **348**, 446 (1980).
- [11] P. Olanders, S.G. Nilsson and P. Möller, *Phys. Lett.* **90 B**, 193 (1980).
- [12] Z. Ma, X. Wu, J. Zhang, Y. Zhuo and J.O. Rasmussen, *Phys. Lett.* **106 B**, 159 (1981).
- [13] F.F. Karpeshin, *Nucl. Phys. A* **617** (1997) 211.
- [14] V.E. Oberacker, A.S. Umar, J.C. Wells, C. Bottcher and M.R. Strayer, *Phys. Lett.* **B293**, 270 (1992).
- [15] V.E. Oberacker, A.S. Umar, J.C. Wells, M.R. Strayer, J.A. Maruhn and P.G. Reinhard, *Proc. Int. Conf. on Fission and Properties of Neutron-Rich Nuclei*, eds J.H. Hamilton and A.V. Ramayya, (Sanibel Island, Florida, USA, November 10–15, 1997), World Scientific (1998), p. 395-404
- [16] V.E. Oberacker, *Heavy-Ion Physics*, Vol. 10, No.2-3, 221-230 (1999)
- [17] W.W. Wilcke, M.W. Johnson, W.U. Schröder, J. R. Huizenga and D. G. Perry, *Phys. Rev. C* **18**, 1452 (1978).
- [18] W.U. Schröder, W.W. Wilcke, M.W. Johnson, D. Hilscher, J. R. Huizenga, J. C. Browne and D. G. Perry, *Phys. Rev. Lett.* **43** (1979) 672.
- [19] S. Ahmad, G.A. Beer, M.S. Dixit, J.A. MacDonald, G.R. Mason, A. Olin, R.M. Pearce, O. Häusser and S.N. Kaplan, *Phys. Lett.* **92B**, 83 (1980).
- [20] S.N. Kaplan *et al.*, in *Proceedings Int. Conf. on Nuclear Physics*, Berkeley, CA (1980), Abstracts (LBL-11118), p. 370.
- [21] Dz. Ganzorig, P.G. Hansen, T. Johansson, B. Jonson, J. Konijn, T. Krogulski, V.D. Kuznetsov, S.M. Polikanov, G. Tibell and L. Westgaard, *Phys. Lett.* **77B**, 257 (1978).
- [22] T. Johansson, J. Konijn, T. Krogulski, S. Polikanov, H.W. Reist and G. Tibell, *Phys. Lett.* **97B**, 29 (1980).

- [23] S. Polikanov, in *Proceedings Int. Summer School on Nuclear Structure*, Dronten, The Netherlands, 1980, (Plenum, New York, 1981), p. 355.
- [24] S. Polikanov, Nucl. Phys. **A502**, 195c (1989).
- [25] F. Risse, W. Bertl, P. David, H. Hänscheid, E. Hermes, J. Konijn, C.T.A.M. de Laat, H. Pruys, Ch. Rösel, W. Schrieder, A. Taal and D. Vermeulen, *Z. Phys. A* **339** (1991) 427.
- [26] E. Fermi and E. Teller, Phys. Rev. **72**, 399 (1947).
- [27] C.S. Wu and L. Wilets, Ann. Rev. Nucl. Sci. **19**, 527 (1969).
- [28] B. Gouillard and H. Primakoff, Phys. Rev. **C 10**, 2034 (1974).
- [29] J.A. Wheeler, Rev. Mod. Phys. **21**, 133 (1949).
- [30] D.F. Zaretski and V.M. Novikov, Nucl. Phys. **28**, 177 (1961).
- [31] B.L. Berman and S.C. Fultz, Rev. Mod. Phys. **47**, 713 (1975).
- [32] A. Neto et al., Phys. Rev. **C18**, 863 (1978).
- [33] E. Teller and M.S. Weiss, *Is the Muon a Multipole Meter?*, Preprint UCRL-83616, Oct. 1979, prepared for the Maurice Goldhaber Festschrift.
- [34] F.F.Karpeshin. J. Phys. **G: Nucl. Part. Phys.** **30** (2004) 1
- [35] Karpeshin F.F., Yad. Fiz., **66**, 1209 (2003); J. Atomic Nuclei (USA), **66**, (2003).
- [36] Yu. N. Demkov, Zh. Eksp. Teor. Fiz. **45**, 195 (1963).
- [37] W.E. Meyerhof, Phys. Rev. Lett. **22**, 1341 (1973).
- [38] Yu.N.Demkov, D.F.Zaretsky, F.F.Karpeshin, M.A.Listengarten, and V.N.Ostrovsky. JETP Lett. **28**, 263 (1978).
- [39] V.A.Karnaukhov. Sov. J. Nucl. Phys. **28**, 621 (1978).
- [40] F.F.Karpeshin and V.N.Ostrovsky. J. Phys. **B: At. Mol. Phys.** **14**, 4513 (1981).
- [41] Karpeshin F.F., Kaschiev M. and Kaschieva V.A. Yad. Fiz., **36**, 336, 1982. (*Engl. transl.* Sov. J. Nucl. Phys. (USA), **36**, 195, 1982.)
- [42] Karpeshin F.F., Kaschiev M. and Kaschiev V.A. Yad. Fiz. 1987, 45, 1556. (*Engl. transl.* Sov. J. Nucl. Phys. 45, 965 (1987))
- [43] L.Bracci and G.Fiorentini, Nucl. Phys. **A423**, 429 (1984)

- [44] F.F.Karpeshin. *J. Phys.* **G16**, 1195 (1990).
- [45] David P., Rösel, Ch., Karpeshin F.F. et al. Proc. of the Workshop on Muonic Atoms and Molecules, Monte Verita, Ascona, April 5 – 9, 1992.
- [46] Karpeshin F.F. *Yad. Fiz.* 55, 29 (1992). (Engl. transl. *Sov. J. Nucl. Phys.* 55, 18 (1992)).
- [47] L.D.Landau and E.M.Lifshitz. *Quantum Mechanics. Nonrelativistic Theory.* Nauka, Moscow, 1974, p. 181.
- [48] D.S.Delion, A.Florescu, and A.Sandulescu. *Phys. Rev.* **C63**, 044312 (2001).
- [49] D.S.Delion, A.Sandulescu and W. Greiner. *J. Phys. G: Nucl. Part. Phys.*, **28**, 2921 (2002).
- [50] K.-J. Bathe. *Numerical Methods in Finite Elements Analysis.* Printice-Hall, Englwood Clif. N.J., 1976.
- [51] D.H.E.Gross and K.M.Hartman. *Phys. Rev.* **C24**, 2526 (1981); P.-G.Reinhard et al. *Phys. Rev.* **C30**, 878 (1984).
- [52] Karpeshin F.F., *Izv. RAN, Ser. Fiz.*, **67**, 710 (2003). (*In Russian*) *Engl. transl.* *Bull. Russian Acad. Sci., Phys. Ser.*, **67**, (2003).
- [53] B.B. Back, *Nucl. Phys.* **A 228** (1974) 323.
- [54] S. Bjornholm and J.E. Lynn, *Rev. Mod. Phys.* **52**, 725 (1980).
- [55] G. Leander and P. Möller, *Phys. Lett.* **57 B**, 245 (1975).
- [56] C. De Boor, *Practical Guide to Splines*, Springer Verlag, New York (1978); and references therein.
- [57] A.S. Umar, J. Wu, M.R. Strayer, and C. Bottcher, *J. Comp. Phys.* **93** (1991) 426.
- [58] A.S. Umar, M.R. Strayer, J.-S. Wu, D.J. Dean, and M.C. Güglü, *Phys. Rev.* **C44**, 2512 (1991).
- [59] J.C. Wells, V.E. Oberacker, M.R. Strayer and A.S. Umar, *Int. J. Mod. Phys.* **C6** (1995) 143
- [60] E. Terán, V.E. Oberacker, and A.S. Umar, *Phys. Rev.* **C 67**, 064314 (2003).
- [61] V.E. Oberacker, A.S. Umar, E. Terán, and A. Blazkiewicz, *Phys. Rev.* **C 68**, 064302 (2003).
- [62] J.A. Diaz et al., *Nucl. Phys.* **40**, 54 (1963).

- [63] B.W. Bush, G.F. Bertsch and B.A. Brown, Phys. Rev. C **45** 1709 (1992).
- [64] D. Kiderlen, H. Hofmann and F.A. Ivanyuk, Nucl. Phys. A (1992).
- [65] C. Wagemans, *The Nuclear Fission Process*, p.418 (CRC Press, Boca Raton, 1991)